




UCT943, a Next-Generation *Plasmodium falciparum* PI4K Inhibitor Preclinical Candidate for the Treatment of Malaria

 Christel Brunschwig,^a Nina Lawrence,^a Dale Taylor,^a Efreem Abay,^a Mathew Njoroge,^a Gregory S. Basarab,^a Claire Le Manach,^b Tanya Paquet,^b Diego González Cabrera,^b Aloysius T. Nchinda,^b Carmen de Kock,^a Lubbe Wiesner,^c Paolo Denti,^c David Waterson,^d Benjamin Blasco,^d Didier Leroy,^d Michael J. Witty,^d Cristina Donini,^d James Duffy,^d Sergio Wittlin,^{e,f} Karen L. White,^g Susan A. Charman,^g Maria Belén Jiménez-Díaz,^h Iñigo Angulo-Barturen,^h Esperanza Herreros,^h Francisco Javier Gamo,^h Rosemary Rochford,ⁱ Dalu Mancama,^j Theresa L. Coetzer,^k Mariëtte E. van der Watt,^l Janette Reader,^l Lyn-Marie Birkholtz,^l Kennan C. Marsh,^m Suresh M. Solapure,^{n†} John E. Burke,^z Jacob A. McPhail,^z Manu Vanaerschot,^o David A. Fidock,^{o,p} Paul V. Fish,^q Peter Siegl,^r Dennis A. Smith,^s Grennady Wirjanata,^t Rintis Noviyanti,^u Ric N. Price,^v Jutta Marfurt,^t Kigbafori D. Silue,^w Leslie J. Street,^b Kelly Chibale^{b,x,y}

^aDrug Discovery and Development Centre (H3D), Division of Clinical Pharmacology, Department of Medicine, University of Cape Town, Observatory, South Africa

^bDrug Discovery and Development Centre (H3D), Department of Chemistry, University of Cape Town, Rondebosch, South Africa

^cDivision of Clinical Pharmacology, Department of Medicine, University of Cape Town, Observatory, South Africa

^dMedicines for Malaria Venture, Geneva, Switzerland

^eSwiss Tropical and Public Health Institute, Basel, Switzerland

^fUniversity of Basel, Basel, Switzerland

^gCentre for Drug Candidate Optimisation, Monash University, Melbourne, Victoria, Australia

^hGlaxoSmithKline, Tres Cantos Medicines Development Campus, Madrid, Spain

ⁱDepartment of Immunology and Microbiology, University of Colorado, Aurora, Colorado, USA

^jBiosciences, Council for Scientific and Industrial Research, Pretoria, South Africa

^kPlasmodium Molecular Research Unit, Wits Research Institute for Malaria, Department of Molecular Medicine and Haematology, School of Pathology, Faculty of Health Sciences, University of the Witwatersrand and National Health Laboratory Service, Johannesburg, South Africa

^lDepartment of Biochemistry, Institute for Sustainable Malaria Control and South African Medical Research Council Collaborating Centre for Malaria Research, University of Pretoria, Pretoria, South Africa

^mAbbVie, North Chicago, Illinois, USA

ⁿNagarjuna Gardens, Bangalore, India

^oDepartment of Microbiology and Immunology, Columbia University Medical Center, New York, New York, USA

^pDivision of Infectious Diseases, Department of Medicine, Columbia University Medical Center, New York, New York, USA

^qAlzheimer's Research UK UCL Drug Discovery Institute, Faculty of Brain Sciences, University College London, London, United Kingdom

^rSiegl Pharma Consulting LLC, Blue Bell, Pennsylvania, USA

^sIndependent Researcher, Walmer, Kent, United Kingdom

^tGlobal and Tropical Health Division, Menzies School of Health Research, Charles Darwin University, Darwin, Australia

^uEijkman Institute for Molecular Biology, Jakarta, Indonesia

^vCentre for Tropical Medicine and Global Health, Nuffield Department of Clinical Medicine, University of Oxford, Oxford, United Kingdom

^wCentre Suisse de Recherches Scientifiques en Côte d'Ivoire, Abidjan, Côte d'Ivoire

^xInstitute of Infectious Disease and Molecular Medicine, University of Cape Town, Rondebosch, South Africa

^ySouth African Medical Research Council Drug Discovery and Development Research Unit, Department of Chemistry, University of Cape Town, Rondebosch, South Africa

^zDepartment of Biochemistry and Microbiology, University of Victoria, Victoria, BC, Canada

Received 23 January 2018 Returned for modification 24 February 2018 Accepted 7 June 2018

Accepted manuscript posted online 25 June 2018

Citation Brunschwig C, Lawrence N, Taylor D, Abay E, Njoroge M, Basarab GS, Le Manach C, Paquet T, Cabrera DG, Nchinda AT, de Kock C, Wiesner L, Denti P, Waterson D, Blasco B, Leroy D, Witty MJ, Donini C, Duffy J, Wittlin S, White KL, Charman SA, Jiménez-Díaz MB, Angulo-Barturen I, Herreros E, Gamo FJ, Rochford R, Mancama D, Coetzer TL, van der Watt ME, Reader J, Birkholtz L-M, Marsh KC, Solapure SM, Burke JE, McPhail JA, Vanaerschot M, Fidock DA, Fish PV, Siegl P, Smith DA, Wirjanata G, Noviyanti R, Price RN, Marfurt J, Silue KD, Street LJ, Chibale K. 2018. UCT943, a next-generation *Plasmodium falciparum* PI4K inhibitor preclinical candidate for the treatment of malaria. *Antimicrob Agents Chemother* 62: e00012-18. <https://doi.org/10.1128/AAC.00012-18>.

Copyright © 2018 American Society for Microbiology. All Rights Reserved. Address correspondence to Kelly Chibale, kelly.chibale@uct.ac.za.

† Deceased.

This paper is dedicated to S. M. Solapure.

ABSTRACT The 2-aminopyridine MMV048 was the first drug candidate inhibiting *Plasmodium* phosphatidylinositol 4-kinase (PI4K), a novel drug target for malaria, to enter clinical development. In an effort to identify the next generation of PI4K inhibitors, the series was optimized to improve properties such as solubility and antiparasitic potency across the parasite life cycle, leading to the 2-aminopyrazine UCT943. The compound displayed higher asexual blood stage, transmission-blocking, and liver stage activities than MMV048 and was more potent against resistant *Plasmodium falciparum* and *Plasmodium vivax* clinical isolates. Excellent *in vitro* antiparasitic activity translated into high efficacy in *Plasmodium berghei* and humanized *P. falciparum* NOD-*scid* IL-2R γ^{null} mouse models. The high passive permeability and high aqueous solubility of UCT943, combined with low to moderate *in vivo* intrinsic clearance, resulted in sustained exposure and high bioavailability in preclinical species. In addition, the predicted human dose for a curative single administration using monkey and dog pharmacokinetics was low, ranging from 50 to 80 mg. As a next-generation *Plasmodium* PI4K inhibitor, UCT943, based on the combined preclinical data, has the potential to form part of a single-exposure radical cure and prophylaxis (SERCaP) to treat, prevent, and block the transmission of malaria.

KEYWORDS 1-phosphatidylinositol 4-kinase inhibitor, absorption, distribution metabolism, excretion, pharmacokinetic/pharmacodynamic modeling, *Plasmodium* spp., drug discovery, human dose prediction, *in vivo* efficacy, malaria, pharmacokinetics

Malaria, an infectious disease transmitted to people through the bite of female *Anopheles* mosquitoes infected with *Plasmodium falciparum* or *Plasmodium vivax*, still afflicts millions of people, with almost 90% of cases on the African continent. Even though the number of malaria cases has fallen globally from an estimated 237 million cases in 2010 to 216 million cases in 2016, malaria still causes 445,000 deaths per year, 99% of which are due to *P. falciparum* in Africa (1). Parasite resistance against currently recommended artemisinin-based combination therapies (2, 3) is a concern, and antimalarial drugs with a novel mode of action are urgently needed. We previously reported the identification of the 2-aminopyridine compound MMV390048 (also known as MMV048), which is efficacious *in vivo* against all measurable *Plasmodium* life cycle stages except hypnozoites (4). MMV048 acts through the inhibition of *Plasmodium* phosphatidylinositol 4-kinase (PI4K) and is the first and sole agent with this mode of action that has entered clinical development. PI4K was reported as a target for *Plasmodium* in 2013 with inhibition by other compound classes (5). The low aqueous solubility associated with MMV048 in biorelevant medium was identified as one of the issues to address in the next generation of PI4K inhibitors along with improved potency. Toward this goal, a scaffold change from the 2-aminopyridine to the 2-aminopyrazine core with concomitant introduction of aqueous solubilizing groups delivered analogues with a better developability profile with respect to improved physicochemical properties, as well as a significant improvement in potency across the parasite life cycle. Improved aqueous solubility was optimally achieved through the incorporation of a piperazinylamide group on the phenyl ring at the 5-position of the 2-aminopyrazine scaffold, leading to UCT943 (Fig. 1). This compound, among other attributes, showed potent *in vitro* activity against multiple stages of the parasite life cycle and excellent *in vivo* efficacy in the *Plasmodium berghei* and *P. falciparum* NSG (NOD-*scid* IL-2R γ^{null}) mouse models (6). In order to assess the potential of UCT943 as a follow-on compound to MMV048 and a preclinical antimalarial candidate, physicochemical, parasitological, and pharmacological profiling was undertaken. Furthermore, extensive drug metabolism and pharmacokinetics (DMPK) profiling was carried out in order to facilitate the prediction of human pharmacokinetic (PK) parameters and the efficacious single dose in humans. The results are reported here.

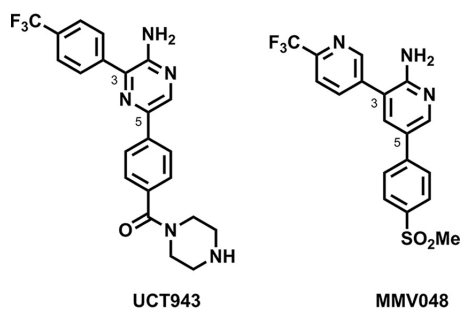


FIG 1 Structures of UCT943 and MMV048.

RESULTS AND DISCUSSION

Rationale for optimization of MMV048 resulting in UCT943. Although MMV048 showed good potency against asexual blood stage parasites, there was room for improvement with respect to activity against liver and the transmissible gametocyte stage parasites (4).

During first-in-human (FIH) studies, MMV048 showed high variability in exposure, which was attributed to low solubility. Intensive and time-consuming formulation work had to be carried out in order to identify a new formulation with a more consistent and 3-fold greater exposure (www.mmv.org/newsroom/interviews/mmv048-0).

To avoid such developability issues in the future, improved solubility, pH dependent and in biorelevant medium, was identified as the main differentiating factor in follow-on compounds. Thus, chemical modifications to MMV048 were made in such a way as to incorporate solubility-enhancing moieties. In this regard, the methyl sulfonyl group of MMV048 was replaced by a water-solubilizing piperazinyl carboxamide on the phenyl ring at the 5-position of the 2-aminopyrazine core to deliver UCT943 (6). Improvements in asexual blood stage and liver stage activities were achieved by replacing the 2-aminopyridine ring with a 2-aminopyrazine ring, which also maintained good potency against gametocytes (6). One key objective of this study was first to determine if these improvements would translate into better *in vivo* efficacy in the *P. falciparum*-infected NSG mouse model and, accordingly, a low predicted human dose.

***In vitro* antiplasmodial activity.** The biological target of the clinical candidate MMV048 was identified to be *Plasmodium* phosphatidylinositol 4-kinase (PI4K) through resistant-mutant generation, sequencing, and pulldown experiments (4). *Plasmodium* PI4K has recently been identified as a new and promising drug target, which is present at all life cycle stages of the *P. falciparum* and *P. vivax* parasites (5). UCT943 inhibits the *P. vivax* PI4K (PvPI4K) enzyme with a 50% inhibitory concentration (IC₅₀) of 23 nM. When tested against a 5-fold-resistant *P. falciparum* strain generated against MMV0489, due to a mutated *pi4k* (*pfpi4k*) locus (4), UCT943 displayed a 6-fold shift in IC₅₀ relative to that of the parental Dd2 strain (14 nM relative to 2.2 nM) (see Table S2 in the supplemental material). When resistance was selected for in Dd2-B2 using UCT943, *pfpi4k* mutants with a 4- or 9-fold IC₅₀ shift were obtained (Table S3). These mutants carried the G1309V or Y1342F mutation, respectively, located in the same region of *pi4k* as MMV048-selected mutations reported elsewhere (4). Resistance selection studies indicated a minimum required inoculum of 10⁷ Dd2 parasites for resistance to emerge, which is similar to that of MMV048 (4). In comparison, IC₅₀ shifts were within 2-fold when UCT943 was tested against strains containing mutated loci in either *pficytB*, *pfhdhdh*, *pfatp4*, or *pfcarl*. These data indicate that UCT943 and MMV048 have the same molecular targets and that, similarly to MMV048, UCT943 is expected to have transmission-blocking and liver stage activities. Importantly, UCT943 maintained high *in vitro* selectivity (>200-fold) for the parasite PvPI4K versus the human PI4Kβ isozyme (IC₅₀ of PI4Kβ, 5.4 μM), inhibition of which is linked to immunosuppressive effects (7).

UCT943 was one of the most potent compounds assessed in the 2-aminopyrazine chemical series (6), with IC₅₀s of 5.4 and 4.7 nM against NF54 and K1 *P. falciparum* strains,

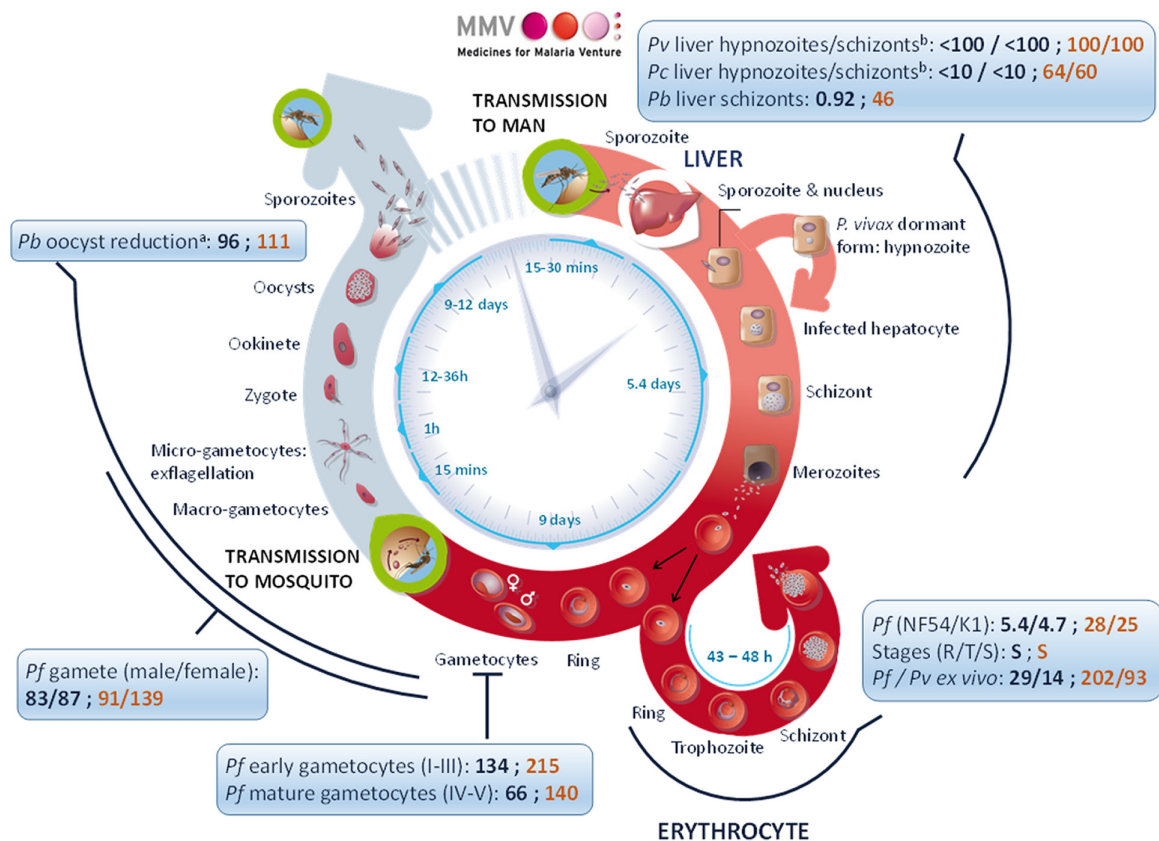


FIG 2 Antiplasmodial activity of UCT943 compared to that of MMV048 against different stages of the parasite life cycle (values indicate IC₅₀s in nanomolar; black, UCT943; brown, MMV048). Values were determined in a standard membrane feeding assay, indirect mode (footnote symbol a) (9), or prophylactic assay (footnote symbol b). *Pf*, *P. falciparum*; *Pb*, *P. berghei*; *Pv*, *P. vivax*; R/T/S, ring/trophozoite/schizont. (Reused with permission from MMV.)

respectively, values that are 5- to 6-fold more active than the IC₅₀s of the clinical candidate MMV048 (4) (Fig. 2). In addition, UCT943 was equally active against the drug-sensitive NF54 strain and multidrug-resistant strains, with IC₅₀s ranging from 4 to 7 nM, thus suggesting that cross-resistance with existing antimalarials is a low risk (Table S1). UCT943 primarily exhibited blood stage activity against schizonts (Table S5), which correlates with a slow rate of kill, as determined in the *in vitro* parasite reduction ratio (PRR) assay (lag phase, 48 h; log PRR, 2.5 at 10× the 50% effective concentration [EC₅₀] in strain 3D7) and in the *in vitro* speed assay (Table S5). As expected, the killing rate profile of UCT943 was similar to that of MMV048 (lag phase, 48 h; log PRR, 2.7) (4). When tested against *P. falciparum* clinical isolates of the Ivory Coast, UCT943 exhibited potent activity (2 to 15 nM) (Table S6). The potency of UCT943 against clinical isolates from Papua, Indonesia, was significantly higher than that of MMV048 in *P. vivax* and in *P. falciparum* (median UCT943 IC₅₀s of 14 nM and 29 nM for *P. vivax* and *P. falciparum*, respectively [*P* = 0.012]; median MMV048 IC₅₀s of 93 nM and 202 nM, respectively [*P* < 0.001]) (Fig. 2 and Table S7). Interestingly, both compounds displayed higher potency against *P. vivax* than against *P. falciparum*, a trend that was also observed for another PI4K inhibitor, KDU691, albeit to a lesser extent (5).

When tested against other stages of the parasite life cycle (Fig. 2), UCT943 was 2 to 50 times more potent than MMV048 (4). UCT943 was potent against early-stage (>90% stages I to III) and late-stage (>95% stages IV and V) gametocytes (IC₅₀s of 134 nM and 66 nM, respectively) and inhibited the formation of both male and female gametes (IC₅₀ of ≈80 nM) in a dual-gamete formation assay (DGFA). The latter activity translated into transmission-blocking activity (target candidate profile TCP5 as defined by Burrows et al. [8]) in a standard membrane feeding assay (SMFA), with an IC₅₀ of 96 nM (9), equivalent to that of MMV048 (Fig. 2). In-depth clinical PK/pharmacodynamic (PD)

TABLE 1 Physicochemical properties of UCT943 and MMV048

Property	Value for the property (SD)	
	UCT943	MMV048
Mol wt (g/mol)	427.4	393.4
LogD (pH 7.4)	−0.27 (0.01)	2.6 (0.03)
pK _a (measured)	7.45 (0.05)	4.0 (0.07)
Thermodynamic solubility (μg/ml) by: ^a		
pH		
2.0	3,000	740
4.0	49	
6.0	110	4.2 (pH 6.5)
8.0	31	4.0 (pH 7.4)
10.0	8.3	
Medium ^b		
SGF (pH 1.8)	5,900	
FaSSIF (pH 6.5)	1,500	14.4
FeSSIF (pH 5.0)	1,900	28.3 (pH 5.8)

^aSingle determination.^bSGF, simulated gastric fluid; FaSSIF, fasted-state simulated intestinal fluid; FeSSIF, fed-state simulated intestinal fluid.

investigations would be needed to determine doses that would afford coverage for both blood stage and transmission-blocking activities. A single drug with both activities would be a valuable addition to the arsenal of antimalarial medicines. UCT943 also exhibits better *in vitro* liver stage activity than MMV048 (potentially addressing TCP3 and TCP4 [8]), targeting schizonts *in vitro* (IC₅₀s of <100 nM and <10 nM in *P. vivax* and *Plasmodium cynomolgi*, respectively, when tested prophylactically, and of 0.92 nM in *P. berghei*), as well as inhibiting the formation of hypnozoites (IC₅₀s of <100 nM and <10 nM in *P. vivax* and *P. cynomolgi*, respectively, when tested prophylactically) (Fig. 2). The parasitophorous vacuole membrane protein UIS4 becomes internalized in MMV048-treated *P. berghei* HepG2 cultures, a morphology associated with *in vitro* liver stage parasite clearance (4). Though UCT943 was not evaluated for such morphological changes, its activity against schizonts offers prospects for improved prophylactic liver stage activity relative to that of MMV048.

Physicochemical characterization. UCT943 was stable in the solid state over a period of 18 months and was chemically stable at 20°C in solutions of dimethyl sulfoxide (DMSO), water (pH 6.2), and buffers (pH 2 and pH 7.4) over 6 days.

The piperazinylamide group accounts for the significantly lower measured lipophilicity of UCT943 (distribution coefficient, logD, of −0.27) than that of MMV048 (logD of 2.6). This, combined with a pK_a of 7.5, results in higher measured solubility in aqueous medium than that of MMV048 across a range of physiologically relevant pHs up to 6.5, where the compound is protonated (Table 1). The compound was also highly soluble in simulated gastric fluid (SGF; pH 1.8), fed-state simulated intestinal fluid (FeSSIF; pH 5.0), and fasted-state simulated intestinal fluid (FaSSIF; pH 6.5) media (>1.5 mg/ml), predictive of a good dissolution in the gastrointestinal tract. The pH-dependent solubility profile of UCT943 in aqueous medium was typical of a weak base with higher solubility at pH below the pK_a, i.e., 7.5 (Fig. 3). UCT943 exhibited high permeability across Caco-2 cells in both directions (apparent permeability, basolateral to apical direction, $P_{app\ B\rightarrow A} = 25 \times 10^{-6}$ cm/s; $P_{app\ A\rightarrow B} = 28 \times 10^{-6}$ cm/s) without appreciable efflux (efflux ratio of 0.93) (Table 2). With high FaSSIF solubility and high permeability, UCT943 can be classified as a developability classification system (DCS) class I compound, which bodes well for a much more favorable development pathway compared to that of MMV048, which was classified as DCS class II (Fig. 4) (10). The high solubility and permeability of UCT943, along with its potent anti-*Plasmodium* activity against all stages of the parasite life cycle (see the section “Rationale for optimization of MMV048 resulting in UCT943”), triggered comprehensive DMPK profiling toward determining its potential for preclinical development.

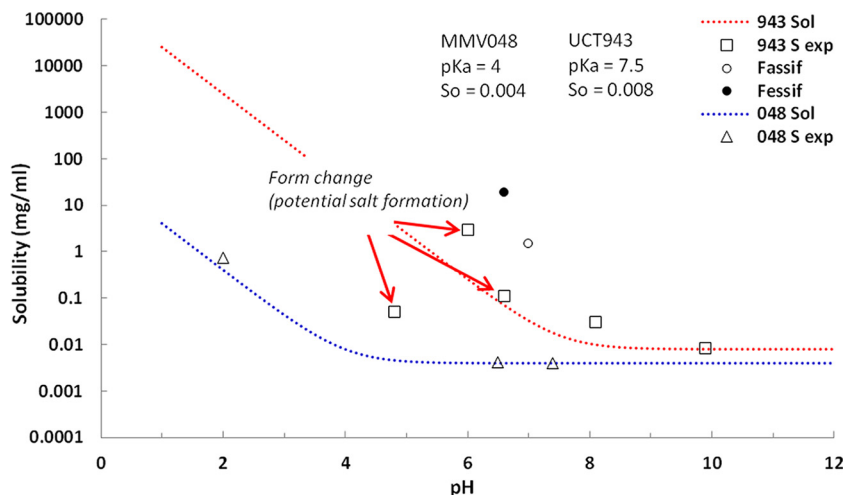


FIG 3 Comparison of pH solubility profiles of MMV048 (048 Sol) and UCT943 (943 Sol). Calculated and measured values for MMV048 (triangle) and UCT943 (square) are indicated. FaSSiF, fasted-state simulated intestinal fluid; FeSSiF, fed-state simulated intestinal fluid.

In vitro and in vivo metabolism studies. There was no evidence of chemical instability for UCT943 in human, dog, rat, or mouse blood or plasma. The compound was moderately bound to plasma proteins with little species differentiation (unbound fraction [f_u] in plasma, 0.10 to 0.16). It also had a greater propensity than MMV048 (blood-to-plasma partitioning ratio [B/P] of ~1.0 across species) to bind or distribute in red blood cells (RBCs) than in plasma (B/P varying from 1.5 to 2.3 across species). This is likely due to enhanced partitioning through the acidic phospholipid bilayer of the cell membrane due to the weakly basic piperazine moiety. The higher partitioning into RBCs possibly contributes to a small degree to its potent *in vitro* and *in vivo* anti-*Plasmodium* activity by localizing the drug where the parasite resides.

As an indicator of hepatic metabolism, UCT943 was incubated across species with hepatocytes, liver microsomes, and liver S9 fractions (Table 2). The intrinsic clearance (CL_{int}) of UCT943 in both microsomes and hepatocytes was low in human, rat, and mouse ($CL_{int} < 11.6 \mu\text{l}/\text{min}/\text{mg}$ in microsomes and $< 4 \mu\text{l}/\text{min}/10^6$ cells in hepatocytes), while it was moderate in dog (CL_{int} 28.2 $\mu\text{l}/\text{min}/\text{mg}$ in microsomes and 9 $\mu\text{l}/\text{min}/10^6$ cells in hepatocytes). Additionally, no significant metabolism ($< 10\%$ degradation) was detected in the human liver S9 fraction, showing that enzymes other than cytochrome P450s (CYPs) were not extensively involved in the metabolism of UCT943. No measurable inhibition was detected at 20 μM against any of the CYP isoforms tested (CYP2D6, CYP2C9, and CYP3A4/5), indicating that UCT943 has low potential for *in vivo* enzyme

TABLE 2 *In vitro* metabolism, protein binding, blood/plasma ratio, and plasma stability data for UCT943^a

Parameter	Value for the parameter (SD) in:			
	Human	Dog	Rat	Mouse
Microsomal CL_{int} ($\mu\text{l}/\text{min}/\text{mg}$)	<11.6 (0.1)	28.2 (0.5)	<11.6 (0.2)	<11.6 (0.7)
Hepatocyte CL_{int} ($\mu\text{l}/\text{min}/10^6$ cells) ^b	<2	9	4	<4
Hepatocyte predicted E_H ^b	<0.2	0.65	0.23	<0.2
f_u microsomes	0.15 (0.01)	0.50 (0.04)	0.45 (0.05)	0.47 (0.04)
f_u plasma	0.17 (0.009)	0.10 (0.007)	0.15 (0.009)	0.10 (0.02)
Blood/plasma ratio	1.5 (0.1)	2.3 (0.1)	2.1 (0.2)	1.9 (0.2)
Plasma stability (after 240 min) (%) ^b	97	95	97	102

^aPermeability across Caco-2 cells in both directions, $P_{app\ B \rightarrow A}$ and $P_{app\ A \rightarrow B}$ was determined as $(25 \pm 5) \times 10^{-6}$ cm/s and $(28 \pm 2) \times 10^{-6}$ cm/s, respectively.

^bSingle determination.

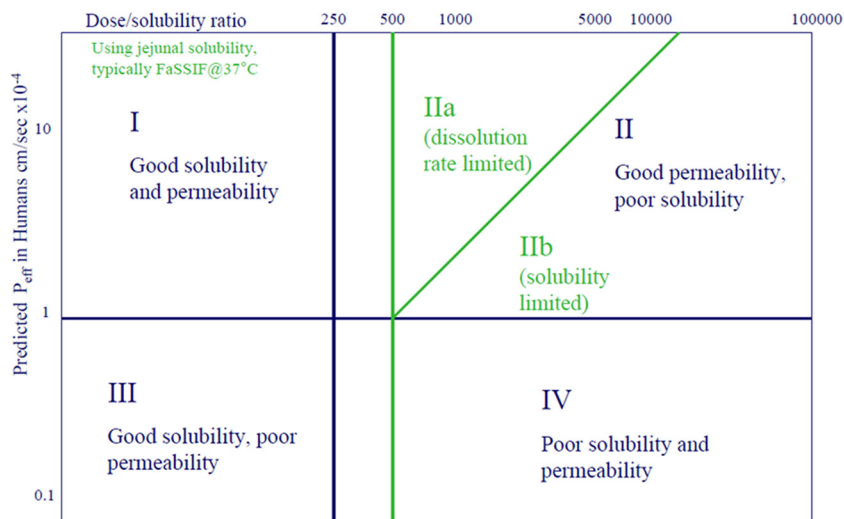


FIG 4 Ranking of UCT943 and MMV048 in the developability classification system (DCS) (10). P_{eff} , effective permeability.

inhibition and that adverse drug-drug interactions through oxidative metabolism are likely to be minimal.

Metabolite identification was performed *in vitro* using liver microsomes and hepatocytes, as well as *in vivo* by analyzing the collected blood samples from mouse PK experiments (Fig. 5a). *In vitro*, liver microsomes and hepatocytes gave a complementary

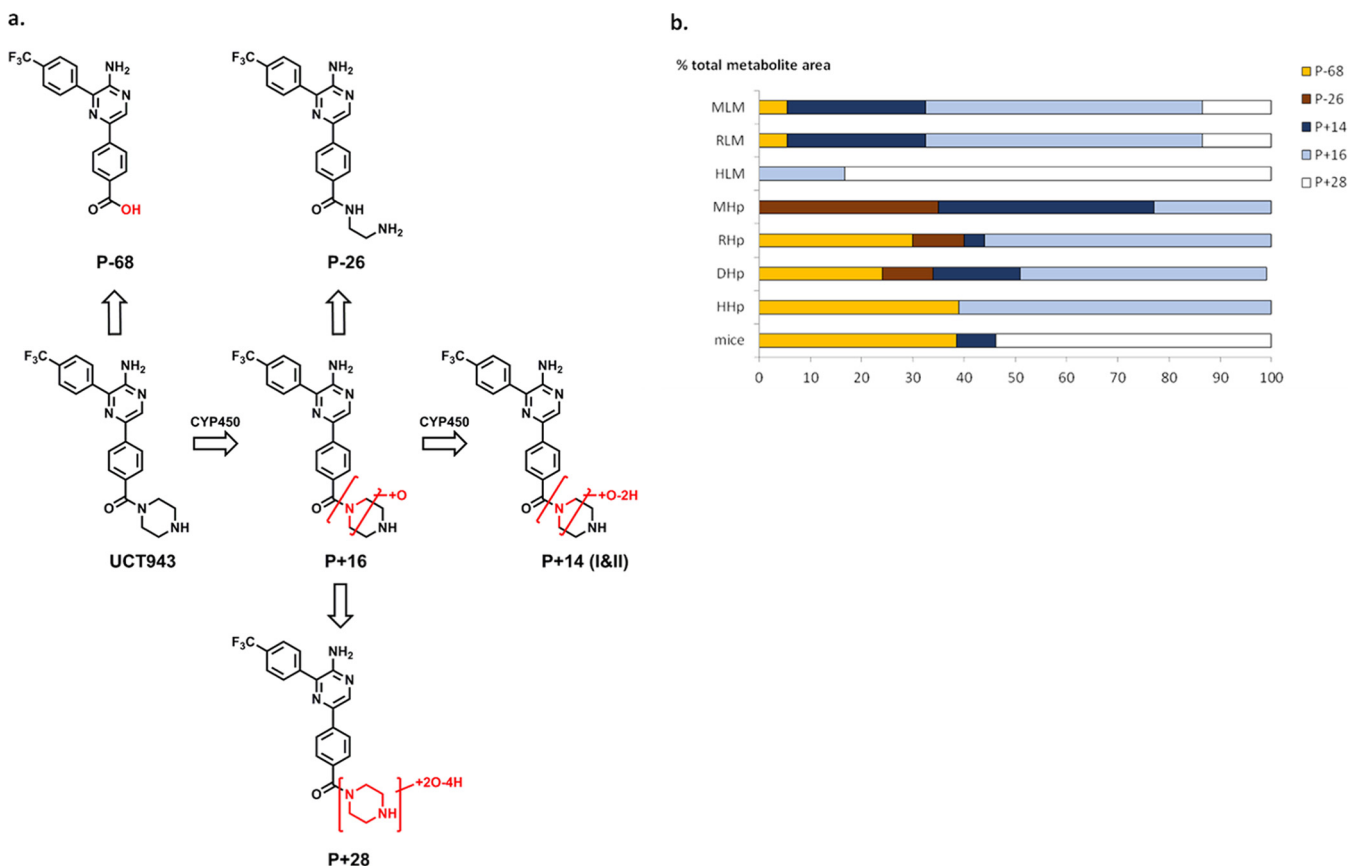


FIG 5 (a) Proposed metabolic pathway of UCT943 in microsomes (mouse, rat, and human) and hepatocytes and *in vivo* in mice. (b) Metabolite profiles of UCT943 in liver microsomes and hepatocytes and in mice. LM, liver microsomes; Hp, hepatocytes; H, human; R, rat; M, mouse; D, dog.

TABLE 3 *In vivo* pharmacokinetic parameters for UCT943 across mouse, rat, dog, and monkey species calculated from noncompartmental analysis

Parameter ^b	Value for the parameter by species and route of drug administration (SD)							
	Mouse		Rat		Dog		Monkey	
	i.v.	p.o.	i.v.	p.o.	i.v.	p.o.	i.v.	p.o.
Dose (mg/kg)	5	20	5	20	2	10	2	10
$t_{1/2}$ (h)	6.4 (0.7)	5.7 (0)	7.4 (0.6)	5.3 (0.3)	13.0	16.1	28.6	34.6
Plasma V_{ss} (liters/kg)	13.1 (1.1) ^a		11.5 (2.1) ^a		7.1 (0.9)		8.7 (1.0)	
CL_b (ml/min/kg)	12.6 (2.4)		9.5 (1.6)		3.3 (0.6) ^a		2.0 (0.3) ^a	
CL_p (ml/min/kg)	24.0 (4.6) ^a		20.0 (3.4) ^a		7.5 (1.2)		3.9 (0.6)	
Plasma $AUC_{0-\infty}$ (min · μ M)	497 (8.5) ^a	1,310 (202) ^a	725 (109) ^a	2,843 (480) ^a	634 (89)	2,335 (754)	1,192 (164)	4,745 (761)
Plasma C_{max} (μ M)	1.2 (0.2) ^a	1.7 (0.3) ^a	2.4 (0.2) ^a	2.1 (0.7) ^a	1.0 (0.1)	2.3 (0.4)	1.5 (0.03)	2.1 (0.4)
T_{max} (h)		4.0 (3.6)		12.0		2.3 (1.5)		7.0 (1.7)
F (%)		66 (10)		98 (4.9)		74 (23.7)		80 (12.8)

^aBlood values were scaled to plasma values using B/P ratios of 1.9, 2.1, 2.3, and 2.0 for mice, rats, dogs, and monkeys, respectively.

^b CL_b , blood clearance; CL_p , plasma clearance; $AUC_{0-\infty}$, area under the concentration-time curve from 0 h to infinity; F , bioavailability.

picture, both showing the major biotransformation pathway occurring on the piperazinylamide moiety (Fig. 5b). UCT943 was mainly metabolized into an oxidation metabolite (P+16), which was further dehydrogenated into two metabolites, P+14 (I and II) in nonhuman species. Further biotransformation on the piperazine ring gave metabolites P-26 (piperazine ring cleavage) and P+28. The formation of the carboxylic acid derivative by hydrolysis of the piperazinylamide moiety (P-68) was more easily detected in hepatocytes and *in vivo* in mice than in liver microsomes, presumably due to the higher concentration of the enzymes responsible for this particular biotransformation. The contribution of these metabolites to the activity of the parent UCT943 is under investigation. Notably, the P-68 metabolite, resulting from the hydrolysis of the carboxamide, showed high activity, albeit lower than that of the parent, with IC_{50} s of 33 nM and 32 nM against *P. falciparum* NF54 and K1 strains, respectively (6).

Pharmacokinetic studies. When administered intravenously, the blood clearance (CL_b) of UCT943 was low in mice, rats, and dogs (Table 3), with a value of less than 20% of hepatic blood flow (11), and very low in monkeys, with a blood CL of <5% of hepatic blood flow, which is consistent with the high *in vitro* metabolic stability. The plasma volume of distribution at steady state (V_{ss}) was high in all species (V_{ss} of 7.1 to 13.1 liters/kg), suggesting that the compound extensively distributes and accumulates in organ tissues. This would be expected for a basic compound due to partitioning into cell membranes by association with acidic phospholipids (12). As a consequence of the low CL and high V_{ss} , half-lives ($t_{1/2}$ s) were long, ranging from 6 h in mice to 29 h in monkeys. When dosed orally in mice and dogs, UCT943 was rapidly absorbed (time of maximum concentration, T_{max} , of <3 h), while absorption in rats and monkeys was slower, with maximum concentrations (C_{max} s) reached after 12 h and 7 h, respectively (Fig. 6). Oral bioavailability was high across all species, ranging from 66% to 98%. The good oral bioavailability and the long $t_{1/2}$ of UCT943 across species are encouraging in terms of the goal of achieving a single-dose treatment and cure for malaria, which would boost patient compliance in resource-limited regions of the world, where the medical infrastructure is not sufficient. If these PK properties are confirmed in humans, UCT943 could thus be a potential combination partner in a single-exposure radical cure and prophylaxis (SERCaP) treatment, as proposed by the Medicines for Malaria Venture (MMV) (8).

***In vivo* efficacy studies.** When dosed at 10 mg/kg *per os* (p.o.), UCT943 reduced parasitemia by >99.9% in the mouse *P. berghei* infection model and cured all mice, with >30 mean survival days (MSD). At 3 mg/kg p.o., no complete cure was achieved, and MSD was 10 days (6), albeit parasitemia was reduced by 99%. The resulting 90% effective dose (ED_{90}) was 1.0 mg/kg p.o. in the *P. berghei* infection model. In the *P. falciparum*-infected NSG mouse model (Fig. S1), UCT943 was 2-fold more potent than MMV048, with an ED_{90} of 0.25 mg/kg for UCT943 and 0.57 mg/kg for MMV048 (4). PK

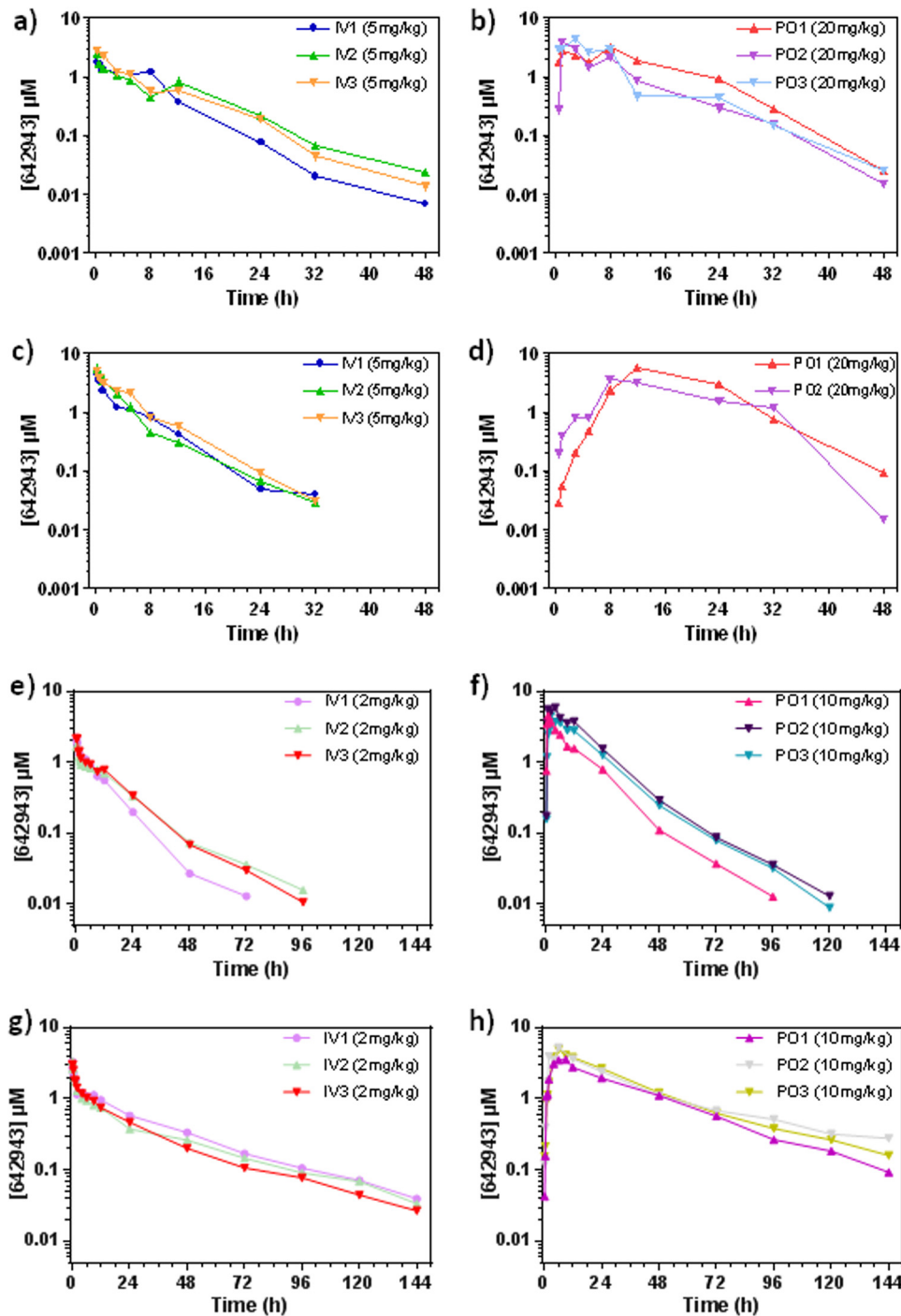


FIG 6 Whole-blood concentration-versus-time profiles following i.v. (left panels) and oral (p.o.) (right panels) administration of UCT943 to nonfasted male BALB/c mice (a and b), fasted male Sprague Dawley rats (c and d), fasted male beagle dogs (e and f), and fasted female *Cynomolgus* monkeys (g and h). 642943, MMV642943 (UCT943). Each line represents results for an individual animal.

data showed that the exposure of UCT943 was dose dependent (6). As PK/PD relationships in the humanized NSG mouse model have been found to be predictive of the induced blood stage malaria (IBSM) model in human volunteers (13), we used the NSG mouse efficacy data for human dose prediction (see the next section).

Prediction of human pharmacokinetics and efficacious single dose by PK/PD modeling. (i) Allometric scaling. The slope used to predict plasma CL by allometric

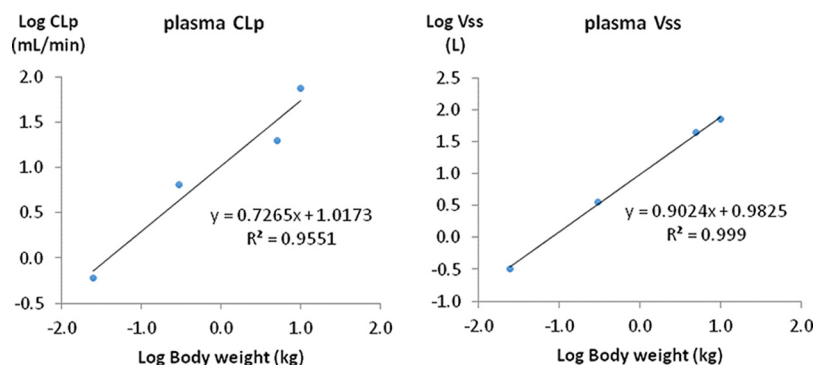


FIG 7 Allometric plots for UCT943 plasma clearance (left) and plasma volume of distribution (right).

scaling was close to 0.75 (0.73), while the slope used to predict plasma V_{ss} was close to 1 (0.90), as expected for metabolic processes and volumes, respectively (14) (Fig. 7). The predicted human plasma V_{ss} was moderately large (6.3 liters/kg), and the predicted human plasma CL was low (0.20 liters/h/kg), as shown in Table 4. When converted using the B/P ratio of 1.5, the predicted human blood clearance was 0.10 liters/h/kg, i.e., less than 10% of liver blood flow (11). The predicted $t_{1/2}$ in humans was 27 h which, together with a long mean residence time of 32 h, suggests that the compound will be a long-duration antimalarial agent.

(ii) Estimation of MPC in blood in the *P. falciparum*-infected NSG mouse model.

From the PK/PD model (Fig. S2 and S3), the compound-specific PD parameters EC_{50} and maximal kill rate constant (K_{kill}) were estimated to be 3.7 ng/ml and 0.060/h, respectively. The minimum parasitocidal concentration in blood (MPC_b), calculated using the EC_{50} , was 7.4 ng/ml in NSG mouse blood and 5.2 ng/ml in human blood (Table 4), after correction for *P. falciparum*-infected NSG mouse and human B/P partitioning data (2.8 and 1.5, respectively). The MPC in plasma (MPC_p) used for human dose prediction was therefore 2.6 ng/ml. The *in vivo* parasite reduction ratio (PRR) of 48 h predicted by the PK/PD model (log PRR of 1.25) correlated closely to the *in vitro* moderate killing profile (log PRR of 2.5), confirming UCT943 as a slow-acting antimalarial compound in this model.

(iii) Prediction of human pharmacokinetic parameters and efficacious dose.

The human PK profiles modeled in the Berkeley Madonna program predicted a single human dose of 50 to 80 mg, based on dog and monkey data, respectively, in order to maintain the plasma concentrations above the predicted therapeutic level (that is, the plasma MPC of 2.6 ng/ml) for 8 days (i.e., four asexual parasite cycles) (Fig. S4 and S5). In this model, a single administration of the efficacious dose to maintain plasma

TABLE 4 Predicted human PK parameters for UCT943 from modeling

Parameter ^a	Value for UCT943
Plasma V_{ss} (liters/kg)	6.3
Plasma CL (liters/h/kg)	0.20
MRT (h)	32
MPC (ng/ml)	
Plasma	2.6
Blood	5.2
k_d (h^{-1})	0.25
F (%)	80
Single dose (mg) ^b	50–80
$t_{1/2}$ (h)	27
Plasma AUC (ng · h/ml)	4,213–8,223
Plasma C_{max} (ng/ml)	234–358

^aMPC, minimum parasitocidal concentration; F, bioavailability.

^bPredicted single dose to achieve ≥ 8 days above the MPC.

TABLE 5 Cytotoxicity and cardiotoxicity data for UCT943 and MMV048^a

Toxicity in cell line or ion channel	CC ₅₀ (SI), μM ^b		
	MMV048	UCT943	UCT943 lowest SI ^c
Cytotoxicity			
CHO cells		17 (3,148)	298
Vero cells		113 (20,926)	1,982
HepG2 cells	>10 (357)	13 (2,407)	225
L6 cells	251 (8,964)	12 (2,222)	211
Cardiotoxicity			
hERG (K _v 11.1)	>11 (393)	10 [6.4–15.9] (1,870)	177
Na _v 1.5	100 (3,571)	>33 (>6,111)	>579
Ca _v 1.2	16 (571)	>33 (>6,111)	>579
K _v 1.5		>33 (>6,111)	>579

^aBoth MMV048 and UCT943 were negative for genotoxicity by the Ames test and micronucleus assay.

^bCC₅₀, 50% cytotoxic concentration; SI, selectivity index. SI is calculated as the CC₅₀/IC₅₀ of strain NF54, where IC₅₀ is the 50% inhibitory concentration. SI values are given as fold change.

^cLowest selectivity index against clinical isolates. The lowest SI is calculated as the CC₅₀/maximum IC₅₀ of the *P. falciparum* clinical isolates.

concentrations above the MPC_p for 8 days resulted in an area under the curve (AUC) of 4,213 to 8,223 ng · h/ml and a predicted C_{max} of 234 to 358 ng/ml, based on monkey and dog, respectively. The low predicted dose is particularly encouraging since it leaves a generous margin for potential dose increases in case the predicted value is underestimated or the dose increase is deemed desirable to prevent the development of resistance or to ensure activity against other malaria species (including *P. vivax*) (see the section above on the rationale for optimization of MMV048).

In vitro cytotoxicity, cardiotoxicity, and genotoxicity. Cytotoxicity, assessed against four mammalian cell lines, was found to be low, with a UCT943 selectivity index (SI) greater than 2,200 relative to the IC₅₀ in NF54 and greater than 170-fold against the highest IC₅₀ in *P. falciparum* clinical isolates (Table 5). The UCT943 SI is equivalent to or greater than that of MMV048. Relative to the predicted upper unbound C_{max} (0.13 μM) for the human efficacious plasma exposure, a 90-fold margin is thereby predicted and is sufficiently high to warrant progression into *in vivo* preclinical toxicology studies.

The safety margins over cardiotoxicity risk were largely improved with UCT943 compared to those with MMV048 (SIs in Table 5). The hERG (ether-à-go-go-related gene) IC₅₀ of 10 μM corresponds to an 80-fold margin relative to the predicted therapeutic unbound C_{max} exposure for efficacy, which indicates a low risk of QT interval prolongation at therapeutic exposures. The margins to potential safety issues associated with potential off-target activities at other ion channels (Na_v1.5, Ca_v1.2, and K_v1.5) are even higher (Table 5).

Genotoxicity was evaluated using the Ames and mouse micronucleus tests, in which UCT943 tested negative at the highest concentrations (Table 5), suggesting that the compound does not have the potential to result in back-mutation of a defective gene to recover its function (Ames test) (15) and does not have the ability to induce the formation of micronuclei during cell division as a consequence of genetic damage (micronucleus assay) (16).

In vivo G6PD hemolysis. In the search for new antimalarial compounds, it is essential to develop drugs which do not pose a red blood cell hemolysis risk to patients with glucose-6-phosphate dehydrogenase (G6PD) deficiency (8). When assessed for *in vivo* hemolytic toxicity in NOD-SCID mice engrafted with A⁻ G6PD-deficient human red blood cells (huRBCs), UCT943 showed day 7 huRBC levels comparable to those of mice treated with the vehicle control, these levels being significantly higher than those of the positive control primaquine (25 mg/kg/day). This indicates that UCT943 does not induce hemolytic toxicity at doses of either 1.5 or 10 mg/kg/day (Fig. S6), which is higher than the ED₉₀ of 0.25 mg/kg in the *P. falciparum* NSG model of infection. Assessment of other markers of hemolysis, including spleen weight and mouse reticu-

locyte levels, also supports the finding that UCT943 did not induce hemolytic toxicity (Fig. S7a and b).

Conclusion. UCT943 was optimized for antiplasmodial activity from a series of 2-aminopyrazines by structural modification of the clinical candidate MMV048, an inhibitor of an essential *Plasmodium* enzyme, PI4K. Incorporation of a piperazinylamide group resulted in enhanced water solubility while maintaining high permeability, both of which are key parameters for a good developability profile and for achieving high drug exposure. This, combined with minimal *in vitro* metabolism in liver subcellular fractions and in hepatocytes, translated into low clearance, sustained exposure, and high bioavailability in preclinical species. UCT943 was potent against all stages of the *Plasmodium* parasite life cycle, as well as against resistant *P. falciparum* and *P. vivax* clinical isolates. The 5-fold increase in *in vitro* antiplasmodial activity of UCT943 compared to that of MMV048 translated into excellent efficacy in the *P. berghei* mouse model and improved efficacy in the humanized *P. falciparum* mouse model. UCT943 was found to be a slow-acting, long-duration antimalarial compound, similar to quinoline antimalarials such as mefloquine. The predicted human single dose using monkey and dog pharmacokinetics was low, ranging from 50 to 80 mg, which offers considerable potential for the drug candidate. The high safety margins over cytotoxicity and cardiac toxicity highlighted here are much larger than the predicted human therapeutic exposure, which is promising. Based on the data presented, UCT943 displays asexual blood stage, transmission-blocking, and liver stage activities and thus has the potential to form part of a single-exposure radical cure and prophylaxis (SERCaP) treatment of uncomplicated malaria. This breadth of activity offers considerable flexibility with respect to treatment options and target product profiles (TPPs) that might be addressed and has contributed to the selection of UCT943 for preclinical development as a follow-on compound to MMV048.

MATERIALS AND METHODS

Chemistry. UCT943 was synthesized in seven steps from commercially available 2-aminopyrazine, as previously described (6).

***In vitro* antiplasmodial activity. (i) Asexual blood stage assays. (a) Cross-resistance against field isolates.** UCT943 was tested using the [³H]hypoxanthine incorporation assay (17, 18) against a panel of drug-sensitive and drug-resistant *P. falciparum* strains (see Table S1 in the supplemental material), as well as against a panel of resistant *P. falciparum* clones generated in the laboratory of David Fidock (Columbia University, USA) (Table S2).

(b) *In vitro P. falciparum* resistance generation to UCT943 and PI4K gene sequencing. The generation of UCT943-resistant *P. falciparum* clones was performed as described elsewhere (4) (Table S4).

(c) *Ex vivo* assay against resistant *P. falciparum* clinical isolates from Côte d'Ivoire. Drug susceptibility of *P. falciparum* isolates from Côte d'Ivoire, West Africa, was measured using incorporation of SYBR green into the parasite's DNA as described before (19). The drug plates contained 10 serial concentrations of the antimalarials, with a maximum concentration of 1,170 nM for UCT943.

(d) *Ex vivo* schizont maturation drug susceptibility assay against *P. vivax* and *P. falciparum* clinical isolates. Drug susceptibility of *P. vivax* and *P. falciparum* isolates from Papua, Indonesia, was measured using a modified schizont maturation assay as described previously (19). The drug plates contained 11 serial concentrations of the antimalarials, with maximum concentrations of 2,993 nM for chloroquine, 1,029 nM for piperazine, 338 nM for mefloquine, 49 nM for artesunate, and 297 nM for UCT943.

(ii) Liver stage assays. (a) *P. berghei* liver stage assay. *Plasmodium berghei* luciferase sporozoites were obtained by dissection of infected *Anopheles stephensi* mosquito salivary glands. A sporozoite invasion assay was performed as described in Le Manach et al. (6) using the rodent parasite *P. berghei*, which is able to infect human hepatocarcinoma HepG2-A16-CD81EGFP cells (20, 21).

(b) *P. cynomolgi* liver stage assay. Primary rhesus hepatocytes were infected *in vitro* with *P. cynomolgi* sporozoites, and the drug assays were performed as previously reported by Zeeman et al. (22).

(c) *P. vivax* liver stage assay. A *P. vivax* liver stage assay was implemented in human hepatocytes infected *in vitro* with *P. vivax* sporozoites, according to the protocol described in Sattabongkot et al. (23).

(iii) Gametocyte assays. *In vitro* gametocytocidal activity was determined using luciferase reporter lines specifically enabling screening against early-stage gametocytes (>90% stages I to III) and late-stage gametocytes (>95% stages IV and V) as per Reader et al. (24). Methylene blue (5 μM) and MMV048 (5 μM) were routinely included as controls.

(iv) *P. falciparum* DGFA. Transmission-blocking activity of UCT943 was assessed in a dual-gamete formation assay (DGFA), which utilizes a dual readout that individually and simultaneously reports on the functional viability of male and female mature stage V gametocytes, as per Ruecker et al. (25).

Physicochemical properties. The pK_a of UCT943 was determined by potentiometric titration as described previously (26). Solubility was measured after 24 h of incubation of solid material with medium at 37°C with residual solids checked by X-ray power diffraction (XRPD). Media included five pH buffers (pH 2.0, 4.0, 6.0, 8.0, and 10.0) and three biorelevant media: simulated gastric fluid (SGF; pH 1.8), fasted-state simulated intestinal fluid (FaSSIF; pH 6.5), and fed-state simulated intestinal fluid (FeSSIF; pH 5.0). Analyses were done by high-performance liquid chromatography (HPLC) (Waters Xbridge C_{18} column, 150 by 4.6 mm, 3- μ m particle size) at 40°C with a mobile phase of 0.1% trifluoroacetic acid (TFA) in water and 0.1% TFA in acetonitrile, with UV detection (220 nm; reference, 500 nm).

In vitro metabolism studies. Metabolic stability of UCT943 (1 μ M) was assessed in human, dog, rat, and mouse liver microsomes using a five-point assay and liquid chromatography-tandem mass spectrometry (LC-MS/MS) as described by Gibhard et al. (27). Metabolic stability (1 μ M) was also evaluated with cryopreserved hepatocytes from the same species (1×10^6 viable cells/ml), as described in Phillips et al. (28). Hepatic extraction ratios (E_H s) were calculated using physiologically based scaling factors as previously described (29).

Binding to plasma proteins and microsomal proteins (0.5 mg/ml) was determined by ultracentrifugation with LC-MS analysis as described in Coteron et al. (30) and Gibhard et al. (27), respectively.

Permeability was determined across Caco-2 monolayers in both apical-to-basolateral and basolateral-to-apical directions using pH 7.4 in both apical and basolateral chambers, as reported in Phillips et al. (19).

Cytochrome P450 (CYP450) inhibition studies (CYP2D6, CYP2C9, and CYP3A4/5) were carried out with pooled human liver microsomes under the conditions described in Walsky and Obach (31). Metabolite identification was performed by LC-MS/MS, as described in Le Manach et al. (32), with a Phenomenex Kinetex PFP (pentafluorophenyl) column (2.1 mm by 100 mm, 2.6- μ m particle size) using microsomal incubations, incubations in hepatocytes from the hepatocyte stability assay, and *in vivo* mouse PK samples.

Plasma stability and whole-blood-to-plasma (B/P) partitioning ratios were determined by spiking blood from humans (Australian Red Cross blood bank), dogs, rats, or mice with UCT943 and incubating samples for 4 h at 37°C. During the incubation period, aliquots of blood were taken to confirm stability. At the end of the incubation period, duplicate aliquots of blood were taken, and the remaining sample was centrifuged to collect duplicate aliquots of plasma. Concentrations in blood and the plasma fraction of blood were measured by LC-MS, and the blood-to-plasma concentration ratio was calculated using the mean concentration for each matrix.

Ethics statement. Animal experiments were approved by the institutional animal care and use committees for each of the experimental sites. All studies were conducted according to the appropriate legislation and respective institutional policies on animal use and welfare.

The human biological samples were sourced ethically, and their research use was in accord with the terms of the informed consents.

Pharmacokinetic studies. Pharmacokinetic studies were performed in mice, rats, dogs, and monkeys as described in the supplemental material. For comparison of blood clearance (CL_b) to hepatic blood flow, values of 90, 55, 31, 44, and 21 ml/min/kg were assumed in mice, rats, dogs, monkeys, and humans, respectively (11).

In vivo efficacy studies. *In vivo* efficacy studies were conducted in the *P. berghei* and *P. falciparum* NOD-*scid* IL-2R γ^{null} (NSG) models as described previously (6, 33; see also the supplemental material).

Prediction of human pharmacokinetics and efficacious single dose by pharmacokinetic/pharmacodynamic (PK/PD) modeling. (i) Allometric scaling. The calculation of human plasma clearance (CL_p) and of human plasma volume of distribution at steady state (V_{ss}) for UCT943 was carried out by a hybrid approach to allometric interspecies scaling (mouse, rat, dog, and monkey) of *in vivo* plasma CL_p and V_{ss} (34). After logarithmic/logarithmic transformation, the parameters were fitted to the equation $\log(y) = \log(a) + b \cdot \log(BW)$, where BW is body weight and a and b are the allometric coefficient and exponent, respectively. Body weights of 0.025, 0.3, 5, 10, and 70 kg were used for mice, rats, monkeys, dogs, and humans, respectively. The mean residence time (MRT) was calculated from the predicted human plasma V_{ss} divided by the predicted human plasma CL_p .

(ii) PK/PD analysis in the *P. falciparum*-infected NSG mouse model to predict MPC. Blood PK data from *P. falciparum*-infected NSG mice were first fitted to a one-compartment model with first-order absorption and elimination. The predicted PK profiles were used to run a direct effect (DE) PK/PD model using Phoenix WinNonlin (Certara, Princeton, NJ) in order to determine the minimum parasitocidal concentration (MPC) of UCT943 (Equations S1 and S2 in the supplemental material).

(iii) Simulation of human PK profiles for human dose prediction. Dog and monkey data were used to predict human PK since higher species allow more extensive blood sampling to explore blood or plasma concentration against time curves in detail. Intravenous (i.v.) and oral (p.o.) time course profiles were normalized in PKSolver (Excel) for preclinical species and Wajima transformed (35). The absorption rate constant (k_a), and the bioavailability (F) estimates were obtained from PKSolver using the Wajima-transformed data. Human p.o. PK parameters were predicted in Berkeley Madonna (University of California, Berkeley, CA) using the Wajima-transformed PK data, the human PK parameters obtained from allometric scaling as described above, and the k_a and F estimates to have the drug concentration above the MPC for ≥ 8 days. The single dose required to maintain the human plasma concentration above the MPC for 8 days (see the previous paragraph) was determined through simulation using the human p.o. PK profiles with Berkeley Madonna.

In vitro cytotoxicity, cardiotoxicity, and genotoxicity. (i) Cytotoxicity. *In vitro* cytotoxicity of UCT943 was tested against L6 cells using the alamarBlue assay and against Chinese hamster ovarian

(CHO), Vero, and HepG2 cells, using an MTT [3-(4,5-dimethyl-2-thiazolyl)-2,5-diphenyl-2H-tetrazolium bromide] assay (36, 37).

(ii) Cardiotoxicity. UCT943 was tested for inhibition of the human ether-à-go-go-related gene (hERG) K⁺ channel (K_v11.1), human K_v1.5 K⁺ channel, and human voltage-gated sodium channel Na_v1.5 using IonWorks patch clamp electrophysiology (38) and for inhibition of the human Ca_v1.2 calcium channel (cardiac L-type) using a fluorescence Ca²⁺ assay. For all assays, 50% cytotoxic concentrations (CC₅₀s) were determined from 8-point dose-response curves generated using 3-fold serial dilutions from the maximum final assay concentration.

(iii) Genotoxicity. (a) Ames. UCT943 was assessed for mutagenic toxicity by measuring its ability to induce reverse mutations in a *Salmonella enterica* serovar Typhimurium-*Escherichia coli*/microsome plate incorporation assay (15, 39). Maximum concentrations were 5,000 μg per plate.

(b) Micronucleus. UCT943 capability to induce clastogenicity/aneugenicity in CHO-WBL cells was determined by measuring the extent of micronucleus formation with and without exogenous metabolic activation (Aroclor 1254-induced rat liver S9). The maximum concentration was 500 μg/ml.

In vivo G6PD hemolysis. *In vivo* hemolytic toxicity was assessed in NOD-SCID mice engrafted with A⁻ glucose-6-phosphate dehydrogenase (G6PD)-deficient human red blood cells (huRBCs) as described in Rochford et al. (40) following a 4-day treatment regimen at dose levels of 1.5 and 10 mg/kg/day given orally.

SUPPLEMENTAL MATERIAL

Supplemental material for this article may be found at <https://doi.org/10.1128/AAC.00012-18>.

SUPPLEMENTAL FILE 1, DOCX file, 0.5 MB.

ACKNOWLEDGMENTS

We acknowledge the following: Nesia Barnes and Warren Olifant from H3D, University of Cape Town (South Africa), for the ADME assays; Virgil Verhoog and Sumaya Salie from H3D, University of Cape Town (South Africa), for the *P. falciparum* blood stage assays; Trevor Finch from the Division of Pharmacology, University of Cape Town (South Africa), for assistance with the animal work; Michael Delves, Andrea Ruecker, and Robert E. Sinden from the Cell and Molecular Biology laboratory, Imperial College, London (United Kingdom), for the gamete formation assay; Anne-Marie Zeeman and Clemens H. M. Kocken from the Biomedical Primate Research Centre, Rijswijk (The Netherlands), for the *P. cynomolgi* *in vitro* prophylactic and radical cure assay; and Rachaneeporn Jenwitisuk from the Faculty of Tropical Medicine, Mahidol University, Bangkok (Thailand), for the *Pv in vitro* prophylactic and radical cure assay.

We acknowledge the Medicines for Malaria Venture (projects MMV09/0002 and 08/0015), Technology Innovation Agency (TIA), the NIH (R01 AI103058 to D.A.F.) and the Strategic Health Innovation Partnerships (SHIP) unit of the South African Medical Research Council (SAMRC) for financial support of this research. K.C. acknowledges support from the University of Cape Town, SAMRC, and South African Research Chairs Initiative of the Department of Science and Technology administered through the National Research Foundation. L.-M.B. and T.L.C. also acknowledge support of SHIP.

REFERENCES

1. WHO. 2017. World malaria report 2017. World Health Organization, Geneva, Switzerland. <http://apps.who.int/iris/bitstream/handle/10665/259492/9789241565523-eng.pdf;jsessionid=2C200E973D697688AB25F51C565B79C4?sequence=1>.
2. Takala-Harrison S, Laufer MK. 2015. Antimalarial drug resistance in Africa: key lessons for the future. *Ann N Y Acad Sci* 1342:62–67. <https://doi.org/10.1111/nyas.12766>.
3. Mbengue A, Bhattacharjee S, Pandharkar T, Liu H, Estiu G, Stahelin RV, Njimoh DL, Ryan Y, Chotivanich K, Nguon C, Ghorbal M, Lopez-Rubio JJ, Pfender M, Emrich S, Mohandas N, Dondorp AM, Wiest O, Haldar K. 2015. A molecular mechanism of artemisinin resistance in *Plasmodium falciparum* malaria. *Nature* 520:683–687. <https://doi.org/10.1038/nature14412>.
4. Paquet T, Le Manach C, González Cabrera D, Younis Y, Henrich PP, Abraham TS, Lee MCS, Basak R, Ghidelli-Disse S, Lafuente-Monasterio MJ, Bantscheff M, Ruecker A, Blagborough AM, Zakutansky SE, Zeeman A-M, White KL, Shackleford DM, Mannila J, Morizzi J, Scheurer C, Angulo-Barturen I, Santos-Martínez M, Ferrer S, Sanz LM, Gamo FJ, Reader J, Botha MJ, Dechering KJ, Sauerwein RW, Tungtaeng A, Vanachayangkul P, Lim CS, Burrows JN, Witty MJ, Marsh KC, Bodenreider C, Rochford R, Solapure SM, Jiménez-Díaz MB, Wittlin S, Charman SA, Donini C, Campo B, Birkholtz L-M, Hanson KK, Drewes G, Kocken CHM, Delves MJ, Leroy D, Fidock DA, Waterson D, Street LJ, Chibale K. 2017. Antimalarial efficacy of MMV390048, an inhibitor of *Plasmodium* phosphatidylinositol 4-kinase. *Sci Transl Med* 9:eaad9735. <https://doi.org/10.1126/scitranslmed.aad9735>.
5. McNamara CW, Lee MCS, Lim CS, Lim SH, Roland J, Nagle A, Simon O, Yeung BKS, Chatterjee AK, McCormack SL, Manary MJ, Zeeman A-M, Dechering KJ, Kumar TRS, Henrich PP, Gagaring K, Ibanez M, Kato N, Kuhen KL, Fischli C, Rottmann M, Plouffe DM, Bursulaya B, Meister S, Rameh L, Trappe J, Haasen D, Timmerman M, Sauerwein RW, Suwanarusk R, Russell B, Renia L, Nosten F, Tully DC, Kocken CHM, Glynn RJ, Bodenreider C, Fidock DA, Diagana TT, Winzeler EA. 2013. Targeting *Plasmodium* PI(4)K to eliminate malaria. *Nature* 504:248–253. <https://doi.org/10.1038/nature12782>.
6. Le Manach C, Nchinda AT, Paquet T, Gonzalez Cabrera D, Younis Y, Han Z, Bashyam S, Zabiulla M, Taylor D, Lawrence N, White KL, Charman SA, Waterson D, Witty MJ, Wittlin S, Botha ME, Nondaba SH, Reader J,

- Birkholtz L-M, Jimenez-Diaz M-B, Santos Martinez M, Ferrer S, Angulo-Barturen I, Meister S, Antonova-Koch Y, Winzeler EA, Street LJ, Chibale K. 2016. Identification of a potential antimalarial drug candidate from a series of 2-aminopyrazines by optimization of aqueous solubility and potency across the parasite life cycle. *J Med Chem* 59:9890–9905. <https://doi.org/10.1021/acs.jmedchem.6b01265>.
7. Lamarche MJ, Borawski J, Bose A, Capacci-Daniel C, Colvin R, Dennehy M, Ding J, Dobler M, Drumm J, Gaither LA, Gao J, Jiang X, Lin K, McKeever U, Puyang X, Raman P, Thohan S, Tommasi R, Wagner K, Xiong X, Zabawa T, Zhu S, Wiedmann B. 2012. Anti-hepatitis C virus activity and toxicity of type III phosphatidylinositol-4-kinase beta inhibitors. *Antimicrob Agents Chemother* 56:5149–5156. <https://doi.org/10.1128/AAC.00946-12>.
 8. Burrows JN, Duparc S, Gutteridge WE, van Huijsduijnen R, Kaszubska W, Macintyre F, Mazzuri S, Möhrle JJ, Wells TNC. 2017. New developments in anti-malarial target candidate and product profiles. *Malar J* 16:26. <https://doi.org/10.1186/s12936-016-1675-x>.
 9. van der Watt M, Reader J, Churchyard A, Nondaba SH, Lauterbach SB, Niemand J, Abayomi S, Van Biljon RA, Connacher JJ, Van Wyk RDJ, Le Manach C, Paquet T, Gonzalez Cabrera D, Brunshwig C, Theron A, Lozano-Arias S, Rodrigues JFI, Herreros E, Leroy D, Duffy J, Street LJ, Chibale K, Mancama D, Coetzee TL, Birkholtz L-M. 2018. Potent *Plasmodium falciparum* gametocytocidal compounds identified by exploring the kinase inhibitor chemical space for dual active antimalarials. *J Antimicrob Chemother* 73:1279–1290. <https://doi.org/10.1093/jac/dky008>.
 10. Butler JM, Dressman JB. 2010. The Developability Classification System: application of biopharmaceutics concepts to formulation development. *J Pharm Sci* 99:4940–4954. <https://doi.org/10.1002/jps.22217>.
 11. Davies B, Morris T. 1993. Physiological parameters in laboratory animals and humans. *Pharm Res* 10:1093–1095. <https://doi.org/10.1023/A:1018943613122>.
 12. Smith DA, Di L, Kerns EH. 2010. The effect of plasma protein binding on *in vivo* efficacy: misconceptions in drug discovery. *Nat Rev Drug Discov* 9:929–939. <https://doi.org/10.1038/nrd3287>.
 13. McCarthy JS, Marquart L, Sekuloski S, Trenholme K, Elliott S, Griffin P, Rockett R, O'Rourke P, Sloots T, Angulo-Barturen I, Ferrer S, Jiménez-Díaz MB, Santos Martinez M, Hooft van Huijsduijnen R, Duparc S, Leroy D, Wells TNC, Baker M, Möhrle JJ. 2016. Linking murine and human *Plasmodium falciparum* challenge models in a translational path for antimalarial drug development. *Antimicrob Agents Chemother* 60:3669–3675. <https://doi.org/10.1128/AAC.02883-15>.
 14. Anderson BJ, Holford NHG. 2008. Mechanism-based concepts of size and maturity in pharmacokinetics. *Annu Rev Pharmacol Toxicol* 48:303–332. <https://doi.org/10.1146/annurev.pharmtox.48.113006.094708>.
 15. Mortelmans K, Zeiger E. 2000. The Ames *Salmonella*/microsome mutagenicity assay. *Mutat Res* 455:29–60. [https://doi.org/10.1016/S0027-5107\(00\)00064-6](https://doi.org/10.1016/S0027-5107(00)00064-6).
 16. Corvi R, Albertini S, Hartung T, Hoffmann S, Maurici D, Pfuhler S, Van Benthem J, Vanparys P. 2008. ECVAM retrospective validation of *in vitro* micronucleus test (MNT). *Mutagenesis* 23:271–283. <https://doi.org/10.1093/mutage/gen010>.
 17. Desjardins RE, Canfield CJ, Haynes JD, Chulay JD. 1979. Quantitative assessment of antimalarial activity *in vitro* by a semiautomated dilution technique. *Antimicrob Agents Chemother* 16:710–718. <https://doi.org/10.1128/AAC.16.6.710>.
 18. Matile H, Richard J, Pink L. 1990. *Plasmodium falciparum* malaria parasite cultures and their use in immunology, p 221–234. In Lefkowitz I, Pernis B (ed), *Immunological methods*, vol IV. Academic Press, San Diego, CA.
 19. Phillips MA, White KL, Kokkonda S, Deng X, White J, El Mazouni F, Marsh K, Tomchick DR, Manjalaranaga K, Rudra KR, Wirjanata G, Noviyanti R, Price RN, Marfurt J, Shackleford DM, Chiu FCK, Campbell M, Jimenez-Diaz MB, Bazaga SF, Angulo-Barturen I, Martinez MS, Lafuente-Monasterio M, Kaminsky W, Silue K, Zeeman A-M, Kocken C, Leroy D, Blasco B, Rossignol E, Rueckle T, Matthews D, Burrows JN, Waterson D, Palmer MJ, Rathod PK, Charman SA. 2016. A triazolopyrimidine-based dihydroorotate dehydrogenase inhibitor with improved drug-like properties for treatment and prevention of malaria. *ACS Infect Dis* 2:945–957. <https://doi.org/10.1021/acsinfecdis.6b00144>.
 20. Silvie O, Rubinstein E, Franetich J-F, Prenant M, Belnoue E, Rénia L, Hannoun L, Eling W, Levy S, Boucheix C, Mazier D. 2003. Hepatocyte CD81 is required for *Plasmodium falciparum* and *Plasmodium yoelii* sporozoite infectivity. *Nat Med* 9:93–96. <https://doi.org/10.1038/nm808>.
 21. Yalauoui S, Zougbedé S, Charrin S, Silvie O, Arduise C, Farhati K, Boucheix C, Mazier D, Rubinstein E, Froissard P. 2008. Hepatocyte permissiveness to *Plasmodium* infection is conveyed by a short and structurally conserved region of the CD81 large extracellular domain. *PLoS Pathog* 4:e1000010. <https://doi.org/10.1371/journal.ppat.1000010>.
 22. Zeeman AM, Van Amsterdam SM, McNamara CW, Voorberg-van Der Wel A, Klooster EJ, Van Den Berg A, Remarque EJ, Plouffe DM, Van Gemert GJ, Luty A, Sauerwein R, Gagaring K, Borboa R, Chen Z, Kuhen K, Glynn RJ, Chatterjee AK, Nagle A, Roland J, Winzeler EA, Leroy D, Campo B, Diagona TT, Yeung BK, Thomas AW, Kocken CH. 2014. KAI407, a potent non-8-aminoquinoline compound that kills *Plasmodium cynomolgi* early dormant liver stage parasites *in vitro*. *Antimicrob Agents Chemother* 58:1586–1595. <https://doi.org/10.1128/AAC.01927-13>.
 23. Sattabongkot J, Yimamnuaychoke N, Leelaudomlpi S, Rasameesoraj M, Jenwithisuk R, Coleman RE, Udomsangpetch R, Cui L, Brewer TG. 2006. Establishment of a human hepatocyte line that supports *in vitro* development of the exo-erythrocytic stages of the malaria parasites *Plasmodium falciparum* and *P. vivax*. *Am J Trop Med Hyg* 74:708–715.
 24. Reader J, Botha M, Theron A, Lauterbach SB, Rossouw C, Engelbrecht D, Wepener M, Smit A, Leroy D, Mancama D, Coetzee TL, Birkholtz L-M. 2015. Nowhere to hide: interrogating different metabolic parameters of *Plasmodium falciparum* gametocytes in a transmission blocking drug discovery pipeline towards malaria elimination. *Malar J* 14:213. <https://doi.org/10.1186/s12936-015-0718-z>.
 25. Ruecker A, Mathias DK, Straschil U, Churcher TS, Dinglasan RR, Leroy D, Sinden RE, Delves MJ. 2014. A male and female gametocyte functional viability assay to identify biologically relevant malaria transmission-blocking drugs. *Antimicrob Agents Chemother* 58:7292–7304. <https://doi.org/10.1128/AAC.03666-14>.
 26. Baragaña B, Hallyburton I, Lee MCS, Norcross NR, Grimaldi R, Otto TD, Proto WR, Blagborough AM, Meister S, Wirjanata G, Ruecker A, Upton LM, Abraham TS, Almeida MJ, Pradhan A, Porzelle A, Martinez MS, Bolscher JM, Woodland A, Luksch T, Norval S, Zuccotto F, Thomas J, Simeons F, Stojanovski L, Osuna-Cabello M, Brock PM, Churcher TS, Sala KA, Zakutansky SE, Jiménez-Díaz MB, Sanz LN, Riley J, Basak R, Campbell M, Avery VM, Sauerwein RW, Decherig KJ, Noviyanti R, Campo B, Frearson JA, Angulo-Barturen I, Ferrer-Bazaga S, Gamo FJ, Wyatt PG, Leroy D, Siegl P, Delves MJ, Kyle DE, Wittlin S, Marfurt J, Price RN, Sinden RE, Winzeler EA, Charman SA, Bebrevska L, Gray DW, Campbell S, Fairlamb AH, Willis PA, Rayner JC, Fidock DA, Read KD, Gilbert IH. 2015. A novel multiple-stage antimalarial agent that inhibits protein synthesis. *Nature* 522:315–320. <https://doi.org/10.1038/nature14451>.
 27. Gibhard L, Pravin K, Abay E, Wilhelm A, Swart K, Lawrence N, Khoury R, van der Westhuizen J, Smith P, Wiesner L. 2016. *In vitro* and *in vivo* pharmacokinetics of aminoalkylated diarylpropanes NP085 and NP102. *Antimicrob Agents Chemother* 60:3065–3069. <https://doi.org/10.1128/AAC.02104-15>.
 28. Phillips MA, Lotharius J, Marsh K, White J, Dayan A, White KL, Njoroge JW, El Mazouni F, Lao Y, Kokkonda S, Tomchick DR, Deng X, Laird T, Bhatia SN, March S, Ng CL, Fidock DA, Wittlin S, Lafuente-Monasterio M, Gamo Benito JF, Sanz Alonso LM, Santos Martinez M, Jimenez-Diaz Maria Belen, Bazaga SF, Angulo-Barturen I, Haselden JN, Louttit J, Cui Y, Sridhar A, Zeeman A-M, Kocken C, Sauerwein R, Decherig K, Avery VM, Duffy S, Delves M, Sinden R, Ruecker A, Wickham KS, Rochford R, Gahagen J, Iyer L, Riccio E, Mirsalis J, Bathhurst I, Rueckle T, Ding X, Campo B, Leroy D, Rogers MJ, Rathod PK, Burrows JN, Charman SA. 2015. A long-duration dihydroorotate dehydrogenase inhibitor (DSM265) for prevention and treatment of malaria. *Sci Transl Med* 7:296ra111. <https://doi.org/10.1126/scitranslmed.aaa6645>.
 29. Ring BJ, Chien JY, Adkison KK, Jones HM, Rowland M, Jones R Do, Yates JWT, Ku MS, Gibson CR, He H, Vuppugalla R, Marathe P, Fischer V, Dutta S, Sinha VK, Björnsson T, Lavé T, Poulin P. 2011. PhRMA CPCDC initiative on predictive models of human pharmacokinetics, part 3: Comparative assessment of prediction methods of human clearance. *J Pharm Sci* 100:4090–4110. <https://doi.org/10.1002/jps.22552>.
 30. Coteron JM, Marco M, Esquivias J, Deng X, White KL, White J, Koltun M, El Mazouni F, Kokkonda S, Katneni K, Bhamidipati R, Shackleford DM, Angulo-Barturen I, Ferrer SB, Jiménez-Díaz MB, Gamo F-J, Goldsmith EJ, Charman WN, Bathurst I, Floyd D, Matthews D, Burrows JN, Rathod PK, Charman SA, Phillips MA. 2011. Structure-guided lead optimization of triazolopyrimidine-ring substituents identifies potent *Plasmodium falciparum* dihydroorotate dehydrogenase inhibitors with clinical candidate potential. *J Med Chem* 54:5540–5561. <https://doi.org/10.1021/jm200592f>.
 31. Walsky RL, Obach RS. 2004. Validated assays for human cytochrome P450 activities. *Drug Metab Dispos* 32:647–660. <https://doi.org/10.1124/dmd.32.6.647>.

32. Le Manach C, Paquet T, Brunschwig C, Njoroge M, Han Z, Gonzalez Cabrera D, Bashyam S, Dhinakaran R, Taylor D, Reader J, Botha M, Churchyard A, Lauterbach S, Coetzer T, Birkholtz L-M, Meister S, Winzeler EA, Waterson D, Witty MJ, Wittlin S, Jimenez-Diaz M-B, Santos Martinez M, Ferrer S, Angulo-Barturen I, Street LJ, Chibale K. 2015. A novel pyrazolopyridine with *in vivo* activity in *Plasmodium berghei*- and *Plasmodium falciparum*-infected mouse models from structure-activity relationship studies around the core of recently identified antimalarial imidazopyridazines. *J Med Chem* 58: 8713–8722. <https://doi.org/10.1021/acs.jmedchem.5b01605>.
33. Jiménez-Díaz MB, Mulet T, Viera S, Gómez V, Garuti H, Ibáñez J, Alvarez-Doval A, Shultz LD, Martínez A, Gargallo-Viola D, Angulo-Barturen I. 2009. Improved murine model of malaria using *Plasmodium falciparum* competent strains and non-myelodepleted NOD-*scid* IL2R γ^{null} mice engrafted with human erythrocytes. *Antimicrob Agents Chemother* 53: 4533–4536. <https://doi.org/10.1128/AAC.00519-09>.
34. Boxenbaum H. 1982. Interspecies scaling, allometry, physiological time, and the ground plan of pharmacokinetics. *J Pharmacokinet Biopharm* 10:201–227. <https://doi.org/10.1007/BF01062336>.
35. Wajima T, Yano Y, Fukumura K, Oguma T. 2004. Prediction of human pharmacokinetic profile in animal scale up based on normalizing time course profiles. *J Pharm Sci* 93:1890–1900. <https://doi.org/10.1002/jps.20099>.
36. Mosmann T. 1983. Rapid colorimetric assay for cellular growth and survival: Application to proliferation and cytotoxicity assays. *J Immunol Methods* 65:55–63. [https://doi.org/10.1016/0022-1759\(83\)90303-4](https://doi.org/10.1016/0022-1759(83)90303-4).
37. Rubinstein LV, Shoemaker RH, Paull KD, Simon RM, Tosini S, Skehan P, Scudiero DA, Monks A, Boyd MR. 1990. Comparison of *in vitro* anticancer-drug-screening data generated with a tetrazolium assay against a diverse panel of human tumor cell lines. *J Natl Cancer Inst* 82:1113–1118. <https://doi.org/10.1093/jnci/82.13.1113>.
38. Schroeder K, Neagle B, Trezise DJ, Worley J. 2003. IonWorks (TM) HT: A new high-throughput electrophysiology measurement platform. *J Biomol Screen* 8:50–64. <https://doi.org/10.1177/1087057102239667>.
39. Mortelmans K, Riccio ES. 2000. The bacterial tryptophan reverse mutation assay with *Escherichia coli* WP2. *Mutat Res* 455:61–69. [https://doi.org/10.1016/S0027-5107\(00\)00076-2](https://doi.org/10.1016/S0027-5107(00)00076-2).
40. Rochford R, Ohrt C, Baresel PC, Campo B, Sampath A, Magill AJ, Tekwani BL, Walker LA. 2013. Humanized mouse model of glucose 6-phosphate dehydrogenase deficiency for *in vivo* assessment of hemolytic toxicity. *Proc Natl Acad Sci U S A* 110:17486–17491. <https://doi.org/10.1073/pnas.1310402110>.